Design and Test of a High-Power High-Efficiency Loosely Coupled Planar Wireless Power Transfer System

Zhen Ning Low, *Student Member, IEEE*, Raul Andres Chinga, *Student Member, IEEE*, Ryan Tseng, and Jenshan Lin, *Senior Member, IEEE*

***Abstract*—In this paper, a high-power high-efficiency wireless-power-transfer system using the class-E operation for transmitter via inductive coupling has been designed and fabricated using the proposed design approach. The system requires no complex external control system but relies on its natural impedance response to achieve the desired power-delivery profile across a wide range of load resistances while maintaining high efficiency to prevent any heating issues. The proposed system consists of multichannels with independent gate drive to control power delivery. The fabricated system is compact and capable of 295 W of power delivery at 75.7% efficiency with forced air cooling and of 69 W of power delivery at 74.2% efficiency with convection cooling. This is the highest power and efficiency of a loosely coupled planar wireless-power-transfer system reported to date.**

***Index Terms*—Class-E, inductive coupling, magnetic induction, switch mode, wireless power transfer.**

I. Introduction

In RECENT years, there has been increasing interest in research and development of wireless power technology [1] to eliminate the "last cable" after Wi-Fi becomes widely accepted. Wireless power systems fall into two main categories: medium to long range, where the coverage is greater or equal to a typical personal-area network, and short range, where the coverage is localized within the vicinity of the transmitting device (typically a 5-in distance). Although there have been attempts [2]–[4] to achieve long-range power delivery via far-field techniques, the efficiency and power delivery is insufficient to legally charge even a typical cellular phone overnight. In order to provide power comparable to a typical wall-mounted dc supply, the system would violate RF safety regulations [5] or has to use a large number of transmitters resulting in an impractical implementation. Therefore, far-field techniques are most suitable for very low power applications unless they are used in less regulated environments such as military or space exploration. Inductive coupling has been one of the leading candidates in achieving wireless power transfer at power levels ranging from several microwatts to several kilowatts. Its operating range is limited as power delivery and efficiency degrades rapidly with increasing distance between the transmitting and receiving unit. Using near-field operation at frequencies below 1 MHz significantly lowers the probability of interference and RF safety issues, since the wavelength is extremely long and radiation is limited. Although harmonics at higher frequencies may be generated, they are filtered by the LC filter network at transmitter output. In addition, the radiation resistance of a small transmitter coil discussed in this paper is still below 0.1 Ω at 10 MHz (tenth or higher harmonics), which makes it a very inefficient loop antenna. Therefore, the radiation of harmonics is very low. The block diagram of the wireless power transfer system using inductive coupling is shown in Fig. 1.

Traditionally, the preferred choice of a driving circuit is the half- or full-bridge inverter [6]–[13] via zero-phase-angle (ZPA) operation. ZPA can be achieved with either frequency control or a variable tank circuit at the transmitter load network. Both techniques can be employed to extend the high efficiency and stable operating range across a wide range of load resistance. Frequency control is preferred over a variable tank circuit because it is significantly more challenging to electronically tune the tank circuit operating at high ac voltage. Recent papers [14], [15] proposed the use of the class-E mode of operation as an alternative. Fundamentally, the class E works with tight operations to achieve zero-voltage switching (ZVS) as well as zero-derivative switching (ZDS). Therefore, it is crucial to keep the operation of the class-E transistor within its operational bounds, as any significant deviation may lead to failure of the transmitter.

Delivering power to a device with a high-efficiency switching regulator at the input of the device can be challenging. This is because a typical buck switching regulator, requiring a higher input voltage to operate, tends to "amplify" the load resistance. The regulator input resistance can be several ohms at a high-power charging state or thousands of ohms during trickle charge state. In addition, developing a robust control system to avoid the bifurcation phenomena [11]–[13] can increase the complexity of the system significantly. Therefore, it is desirable for the wireless power system to have a natural response without any external control or feedback such that its power-delivery property closely matches a typical wall-mounted dc supply and is transparent to the device.

Manuscript received June 6, 2008; revised October 28, 2008. First published December 2, 2008; current version published April 29, 2009. This work was supported in part by WiPower Inc. and in part by the Florida High Tech Corridor Council.

Z. N. Low, R. A. Chinga, and J. Lin are with the Electrical and Computer Engineering Department, University of Florida, Gainesville, FL 32611 USA (e-mail: znlow@ufl.edu).

R. Tseng is with WiPower Inc., Gainesville, FL 32641 USA (e-mail: rtseng@wipower.com).

Color versions of one or more of the figures in this paper are available online at http://ieeexplore.ieee.org.

Digital Object Identifier 10.1109/TIE.2008.2010110

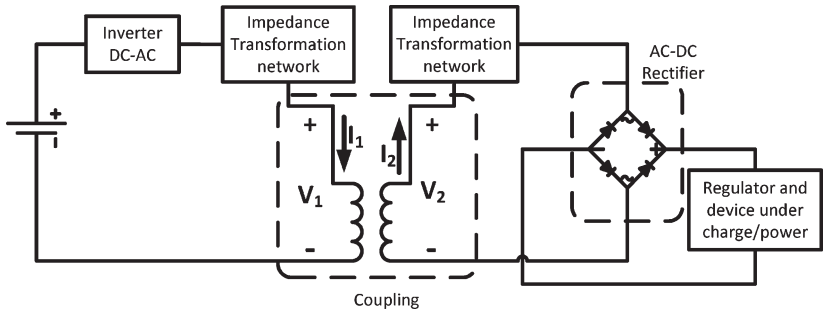

Fig. 1. Block diagram of the wireless power transfer system using inductive coupling.

Although it is important to achieve high efficiency, it is also crucial to ensure that the system is able to deliver the required power with respect to the load resistance. The transmitted power should decrease when the load impedance increases. Error in selecting component values will result in the opposite direction of operation, i.e., the transmitter will increase its output when the load resistance increases. The switching regulator will attempt to maintain its power delivery by increasing its input resistance or decrease its duty cycle, resulting in a positive feedback. Poor efficiency will be observed due to excess power dissipated as heat, and device failure may occur due to overvoltage.

In addition, a robust wireless power transfer system must be able to provide a significant amount of translational freedom such that the power transfer is insensitive to the placement of the device. This convenience for users of portable wireless devices is the key feature of the proposed wireless power transfer system. Therefore, the receiving coil should be significantly smaller than the transmitting coil, resulting in coupling that is generally weak/loose with a coupling coefficient of less than 0.5. Under this condition, the interaction between the coils cannot be treated like an ideal transformer.

In this paper, a design approach is proposed to realize an efficient wireless power transfer system achieving low-power loss using the class-E mode of operation. In addition, the system is able to achieve a desirable power-delivery response across a wide range of load resistances without any control mechanism or feedback loop. An efficient compact wireless power system achieving 295 W of power delivery with better than 75% end-to-end dc-to-dc conversion efficiency across the main power-delivery impedance range is developed to verify the design approach. The system can be used to provide power wirelessly to various portable devices for consumer electronics, industrial appliances, and many other applications.

II. Analysis of Operation

A. Inductive Coupling

Power transfer for the system is achieved via magnetic induction between two air core coils. Appropriate shielding [16] at the expense of weight and thickness can be used to make the system more robust in environments where the system's magnetic field is likely to interact with other nearby objects. However, shielding is beyond the scope of this paper, and it is assumed that the system will be working in an environment free of structures and materials that will significantly affect the system performance.

Although it would be ideal for both the transmitting coil and the receiving coil to be of the same size to ensure maximum coupling, a practical system uses a receiver coil significantly smaller than the transmitting coil. This allows a user to freely place a device in any orientation as shown in Fig. 16. Therefore, in order to achieve consistent power delivery regardless of the receiving coil's location, the transmitting coil must be able to generate a magnetic field that has relatively even distribution. This can be achieved by using the method proposed in [17] and [18].

The voltage and current characteristics of the transmitting and the receiving coils can be described using the following [6], [11]:

$$V_1 = j\omega M_{11} I_1 + j\omega M_{12} I_2 \tag{1}$$

$$V_2 = j\omega M_{21} I_1 + j\omega M_{22} I_2 \tag{2}$$

$$M_{12} = k\sqrt{M_{11} M_{22}} \tag{3}$$

where

V_1	voltage at the transmitting coil (Fig. 1);
I_1	current at the transmitting coil (Fig. 1);
V_2	voltage at the receiving coil (Fig. 1);
I_2	current at the receiving coil (Fig. 1);
M_{11}	self-inductance of the transmitting coil;
M_{22}	self-inductance of the receiving coil;
$M_{12} = M_{21}$	mutual inductance of the two coils;
k	coupling coefficient between the two coils.

By Ohm's law,

$$Z_{tx} = R_{tx} + jX_{tx} = \frac{V_1}{I_1} \tag{4}$$

$$Z_{rx} = R_{rx} + jX_{rx} = \frac{V_2}{I_2}. \tag{5}$$

Using (1), (2), and (4) and assuming a time-harmonic operation with frequency ω,

$$Z_{tx} = \frac{\omega^2 M_{12}^2 R_{rx}}{R_{rx}^2 + (\omega M_{22} + X_{rx})^2} + j\left(\omega M_{11} - \frac{\omega^2 M_{12}^2 (\omega M_{22} + X_{rx})}{R_{rx}^2 + (\omega M_{22} + X_{rx})^2}\right). \tag{6}$$

The earlier analysis of the coupling neglects any second-order effects such as skin depth and proximity effects. A

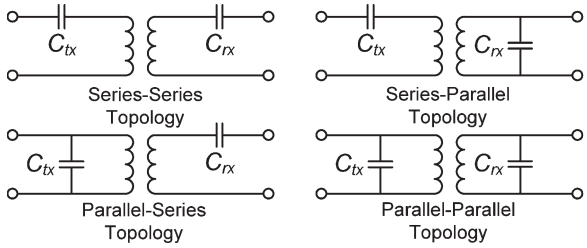

Fig. 2. Topologies for a single-element impedance transformation network.

more in-depth analysis accounting for the earlier effects can be performed to improve the accuracy. Alternatively, Litz wires can be used to mitigate such effects.

B. Impedance Transformation Network

The purpose of impedance transformation networks on the primary and secondary sides of the coupling is to achieve maximum power transmission and efficiency by operating within the optimum impedance range looking into the transmitter load network [19] over a wide range of load resistance.

In consideration of size and efficiency, capacitors instead of resistors and inductors should be used for the network. This is because resistors dissipate power, and the size of a low-loss inductor is generally large. Although a multielement transformation network might achieve a better response, for simplicity and low-component count, the system uses a single-element transformation network. The four possible topologies of the single-element transformation network are shown in Fig. 2.

Fundamentally, a series capacitor only introduces a negative reactance and does not change the real part of the impedance. On the other hand, a parallel capacitor changes both the real and imaginary parts of the impedance. To simplify the analysis, the receiver input impedance is modeled using a variable resistor load, and (7) illustrates the transformation performed by the parallel capacitor

$$Z_{rx} = \frac{R}{1+\omega^2 C^2 R^2} - j\frac{\omega C R^2}{1+\omega^2 C^2 R^2}. \tag{7}$$

Equation (7) shows that the resistance R_{rx} is "compressed" by a factor of $1/(1+\omega^2 C^2 R^2)$. Thus, the equivalent resistance R_{rx} decreases with increasing load resistance. At high load resistance, the transformed resistance is small. Therefore, a significant part of the received power is dissipated across the receiving coil as heat. This phenomenon is desirable if the receiver is in a state that requires very little power or during trickle charge. Therefore, it has a "decoupling" effect regulating the power delivery with increasing load resistance. However, this should occur if, and only if, the transmitter is designed to output limited power under this operation condition because heating can become a problem if too much power is being dissipated across the receiving coil. Due to the parallel capacitor, a reactive term jX_{rx} is introduced. The reactive term decreases nonlinearly from null with increasing load resistance with an asymptote of $-1/\omega C$. This can be useful to compensate the receiving-coil inductance.

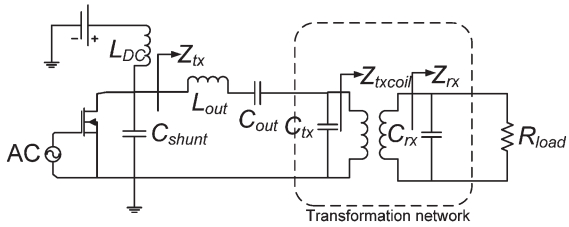

Fig. 3. Simplified schematic of wireless power transfer system using parallel–parallel transformation network and class-E transmitter. Z_{tx}—Impedance looking into the transmitter load network. $Z_{tx\mathrm{coil}}$—Impedance looking into the transmitting coil. Z_{rx}—Impedance looking into receiver network. R_{load} is the equivalent resistance looking into the rectifier.

From (6), it can be observed that the resistance looking into the transmitter coil R_{tx} is reduced significantly if the resistance looking from the receiver coil into the receiver R_{rx} is increased. Due to loose coupling between the coils, R_{tx} is further reduced because the mutual inductance is relatively small. If the total resistance looking into the transmitting coil is mainly the parasitic resistance of the transmitting coil, limited power is transmitted to the receiver as most of the power is dissipated across the transmitting coil as heat. Therefore, it is preferred for a wireless power-transmission system using loosely coupled coils to have a parallel capacitor on the receiving coil. By substituting (7) into (6), the expression of impedance looking into the transmitting coil with a parallel capacitor across the receiving coil is

$$Z_{tx} = \left(\frac{\omega^2 M_{12}^2\left(\frac{R}{1+\omega^2C^2R^2}\right)}{\left(\frac{R}{1+\omega^2C^2R^2}\right)^2+\left(\omega M_{22}-\frac{\omega CR^2}{1+\omega^2C^2R^2}\right)^2}\right) + j\left(\omega M_{11}-\frac{\omega^2 M_{12}^2\left(\omega M_{22}-\frac{\omega CR^2}{1+\omega^2C^2R^2}\right)}{\left(\frac{R}{1+\omega^2C^2R^2}\right)^2+\left(\omega M_{22}-\frac{\omega CR^2}{1+\omega^2C^2R^2}\right)^2}\right). \tag{8}$$

For the transmitter transformation network, a series or parallel topology can be used. However, to maintain an ideal efficiency above 95%, the allowable variation of load resistance of an ideal class-E amplifier should be kept within $+55\%$ and -37% [19]. Therefore, if the variation is too large, it is preferred that a parallel capacitor is used instead of a series capacitor to "compress" the resistance. A suitable capacitor value is needed to ensure that the transmitter does not suffer immediate failure when there is no receiving coil and to produce an increasing reactance trend with increasing load resistance so as to ensure the preferred power-delivery trend. Based on the earlier analysis, the parallel–parallel topology is chosen for the system.

C. Class-E Transmitter

The switched-mode class-E transmitter shown in Fig. 3 is selected over the popular class-D transmitter for this application due to its simplicity and high-efficiency operation. Although it is known that class-E operation requires its switching transistor to have a $3.562\times$ higher breakdown voltage than that of the class D, it is often overlooked that the output power of

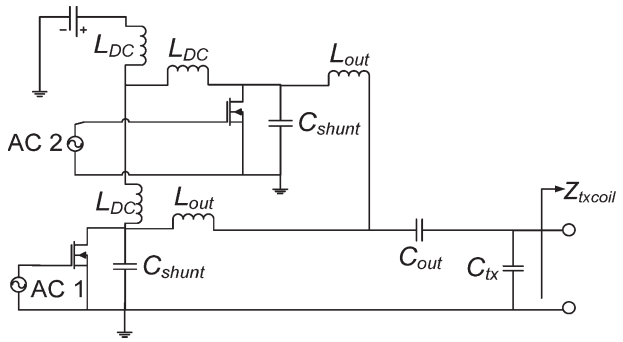

Fig. 4. Schematic of the dual-channel class-E transmitter.

an optimized ideal single-ended class-E transmitter as shown in (9) is 2.847× higher than that of typical optimized ideal class-D transmitter as shown in (10)

$$P_{\text{out-class-E}} = \frac{8}{\pi^2+4}\frac{V_{CC}^2}{R} = 0.5768\left(\frac{V_{CC}^2}{R}\right) \quad (9)$$

$$P_{\text{out-class-D}} = \frac{2}{\pi^2}\frac{V_{CC}^2}{R} = 0.2026\left(\frac{V_{CC}^2}{R}\right). \quad (10)$$

From (9) and (10), we can conclude that, in order to achieve similar output power, the class D requires a supply voltage that is 1.687× higher than that of class E. When supply voltage is constrained, a class-E transmitter is preferred to a class-D transmitter because of higher output power at the same supply voltage. In addition, the single-transistor (class E) topology which only requires a single clock source is used instead of the dual-transistor (class D) topology that would require a pair of out-of-phase gate drive. The class-E topology decreases the complexity considerably.

In addition to the typical single-ended class-E transmitter, a dual-channel class-E transmitter with independent gate drive shown in Fig. 4 is also designed. It is shown in Section IV that the efficiency degrades significantly during low power consumption or trickle-charge mode as the load resistance at receiver R_{load} becomes too large. Therefore, the dual-channel class E allows the system to shutdown one of the channels to switch to a lower power mode so that the receiver's regulator responds by reducing its input resistance, such that the system efficiency is increased by approximately 15%. The analysis of the dual-channel class E is straightforward. If both the channels are enabled, the equivalent inductance across both L_{out} is $L_{\text{out}}/2$, while if one channel is enabled, the equivalent inductance is simply L_{out}. Likewise, the equivalent value of C_{shunt} is doubled for a dual-channel configuration. The dual-channel class-E transmitter can be easily scaled to multiple channels but the size increases along with a higher probability of device mismatches. As the number of channels increases, the problems caused by device mismatches might far outweigh the benefits. It was found empirically that the number of channels should be kept at a maximum of three. The observed efficiency improvement was negligible when the number of channels was increased from three to four, and the efficiency started to degrade at five channels, predominately due to variations in inductance value. Although this technique enables the system to operate at a higher efficiency, the tradeoff is that the power delivered to the load network is fed across a single inductor instead of two. Thus, the equivalent parasitic resistance of L_{out} is doubled for a dual-channel topology, reducing the potential enhancement of the system efficiency.

III. Design Approach

The design of the proposed wireless power system is started by setting constraints of the dimensions of the transmitting and receiving coils as well as operating frequency. The following analysis is based on the dual-channel transmitter topology. It can be reduced into a single-channel or extended to multiple channels. Although higher operating frequency is preferred to shrink the components, switching and parasitic losses might become too high. An operating frequency of 134 kHz is used for all of the analysis in this paper. To simplify the analysis, the load resistance is defined as the equivalent resistance looking into the rectifier instead of after the rectifier. It is desirable for the receiving coil to be much smaller than the transmitting coil, but the efficiency and power-transfer capabilities start to degrade significantly due to poor coupling if the receiver is too small. The effective resistance looking into the transmitting coil is related to the mutual induction by a square-law effect as shown in (6). The mutual inductance is related to the coupling coefficient by a factor of the square root of the self-inductances of both coils as shown in (3). Therefore, the effective resistance looking into the coil decreases rapidly with decreasing coupling coefficient k. Therefore, the parasitic resistance of the transmitting coil becomes significant with decreasing effective resistance looking into the transmitting coil and may cause undesired heating. It is found empirically that a coupling coefficient k above 0.25 is desirable to mitigate any heating issues or significant degradation in efficiency. To minimize space usage as well as ease of integration into the target device, the receiving coil is typically tightly wound. However, the windings of the transmitting coil are very different from the receiving coil. The gaps between each turn of the transmitting coil are spaced in a manner to achieve even field distribution and consistent performance regardless of the placement of receiving coil. An example can be found in [21].

Key parameters of the coils including self-inductances, mutual inductance, and parasitic resistances can be extracted by measuring the fabricated coil with an impedance analyzer or analyzing with electromagnetic simulation tools.

A. Determination of C_{rx} Value

The design of the system starts from the receiver looking into the load. The typical impedance response for different parallel capacitors is shown in Fig. 5.

The capacitance value is selected based on the inductance of the receiving coil as well as the mutual inductance between the coils. It is ideal to achieve a maximum resistance looking into the transmitting coil across a wide range of load resistances. However, in reality, the optimum capacitance value is different for different load resistances. In addition, there is no closed-form analytical solution. Differentiating the real part of (8) and solving for the optimum receiver-capacitance value is

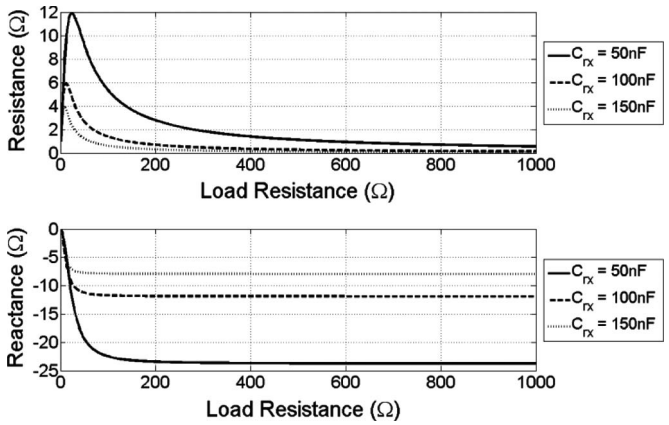

Fig. 5. Resistance and reactance of Z_{rx} versus load resistance at different with different C_{rx} (50, 100, and 150 nF).

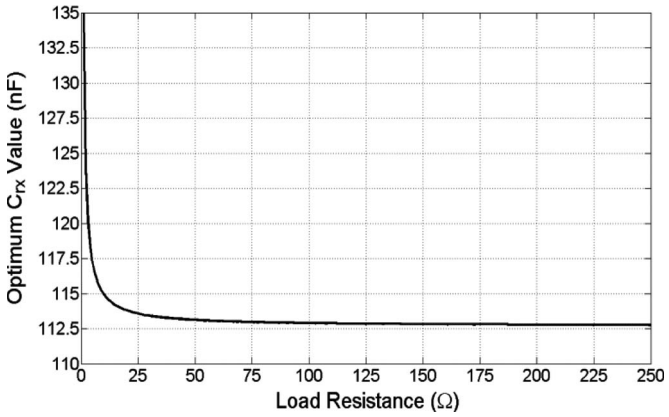

Fig. 6. Optimum receiver capacitor value versus load resistance.

not straightforward. Therefore, a simple parameter sweep of MATLAB code is used to sweep through a range of receiver resistance and capacitance values to extract the optimum value. A pair of coils was fabricated using 16 AWG magnetic wires for the experiment. The transmitting coil is 21 cm by 21 cm with ten turns while the receiving coil is 13 cm by 13 cm with five turns tightly wounded together. The transmitting coil is designed with the appropriate spacing between the turns to achieve 5% variation of the received power at all different locations. Therefore, it can be reasonably assumed that the coupling is constant regardless of receiving-coil position. The self-inductance of the transmitting coil is 31.95 μH with a parasitic resistance of 0.32 Ω. The receiving coil is 12.52 μH with a parasitic resistance of 0.2 Ω. Mutual inductance between the coils is 7.454 μH with a coupling coefficient of 0.373. Both of the coils were measured using the HP4192A LF Impedance Analyzer.

Based on the coil parameters, Fig. 6 shows the optimum C_{rx} value versus load resistance. The optimum C_{rx} value decreases rapidly from 135 to 113 nF with increasing load resistance. The typical operation of a switching voltage regulator used for this application does not present a very low resistance at its input. Therefore, it can be safely concluded that to power a typical USB-enabled device at 5 V, 500 mA (input resistance of 10 Ω), the regulator input resistance should not drop below 25 Ω by assuming that the regulator has a 100% efficiency

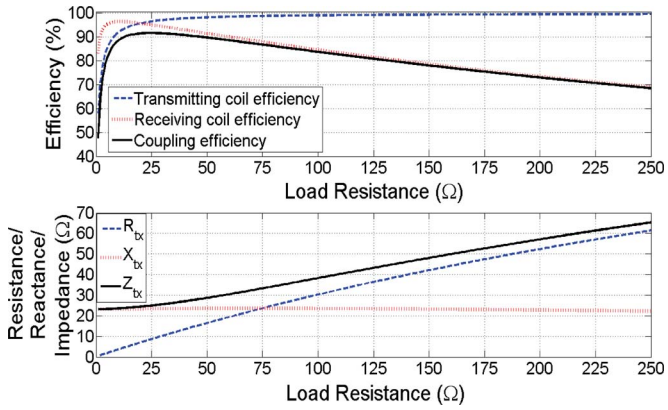

Fig. 7. Coupling efficiency and transformed impedance looking into the transmitting coil.

and the minimum input regulation voltage is 8 V. In addition, it is likely that the regulator will operate with load resistance between 25 and 100 Ω during high-power-transfer state for a portable device such as a cellular phone, mp3 player, camera, etc. Therefore, it is important to achieve high efficiency across this impedance range. Therefore, 113 nF is chosen as the preferred receiver-capacitance value.

Fig. 7 shows the coupling efficiency k between the coils and the impedance looking into the transmitting coil $(Z_{tx\text{coil}})$. The efficiency is calculated using the ratio of the power delivered to the resistance R_{tx} over the power delivered to both the parasitic resistance and the effective resistance R_{tx}. The earlier method is used to determine the transmitting- and receiving-coil efficiencies. The coupling efficiency is the combination of both the transmitting- and receiving-coil efficiencies. It can be seen that the efficiency of the transmitting coil remains high for all cases, which is desirable. This is because the transmitter puts out a large amount of power and should have a higher efficiency to mitigate heat loss. The gradual degradation in receiver efficiency is desirable as it helps to regulate the power during trickle charge. This can be seen in later analysis that the power delivered by the transmitter remains consistent at high load resistances. This is because the equivalent load impedance Z_{tx} looking into the transmitter load network does not change much.

B. Determination of C_{tx} Value

Selecting an appropriate transmitting-coil parallel-capacitor value needs to fulfill two constraints. First, the system must not fail catastrophically when the receiving coil is removed from the transmitting coil. Although it is possible to implement a load-detection scheme to turn off the transmitter and reduce unloaded power losses, it is still desirable for the unloaded power consumption to be minimal. Since the coil voltage is unique to each load resistance as shown in Fig. 8, load detection and status can be easily acquired. To avoid false detection, the load detection and status can be verified by analyzing the supply current via a current-sense resistor.

Limiting unloaded power loss can be achieved by ensuring that the unloaded Z_{tx} has equivalent impedance similar to the case with a high load resistance (high impedance with large

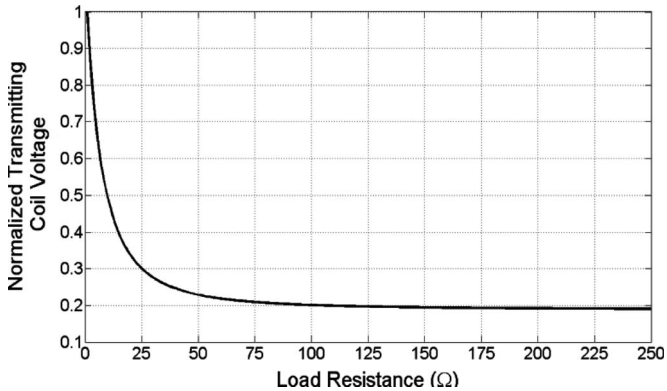

Fig. 8. Normalized transmitting-coil voltage versus load resistance.

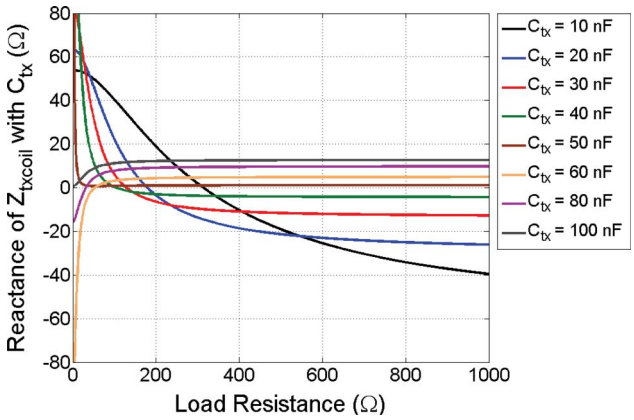

Fig. 9. Reactance of Z_{txcoil} versus load resistance with different C_{tx}.

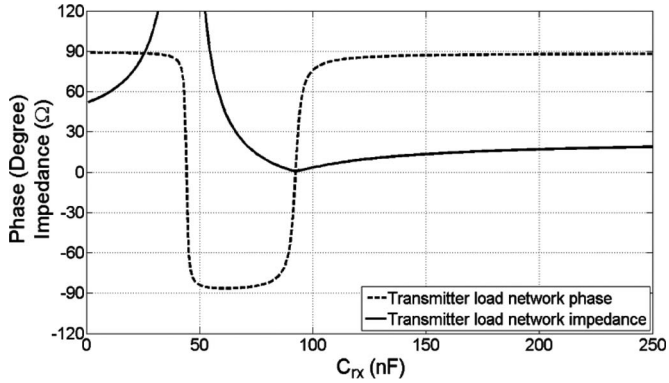

Fig. 10. Amplitude and phase of impedance of unloaded Z_{tx} versus C_{tx}.

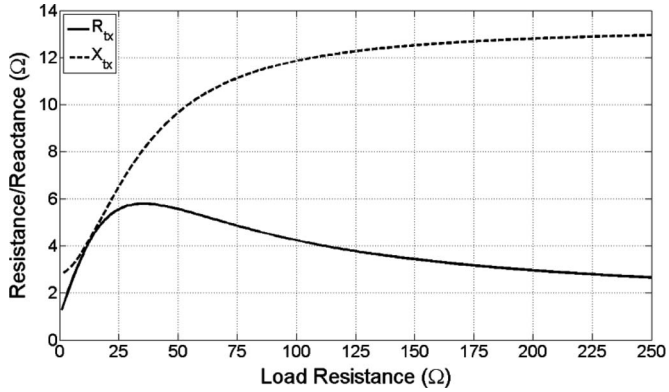

Fig. 11. R_{tx} and X_{tx} versus load resistance.

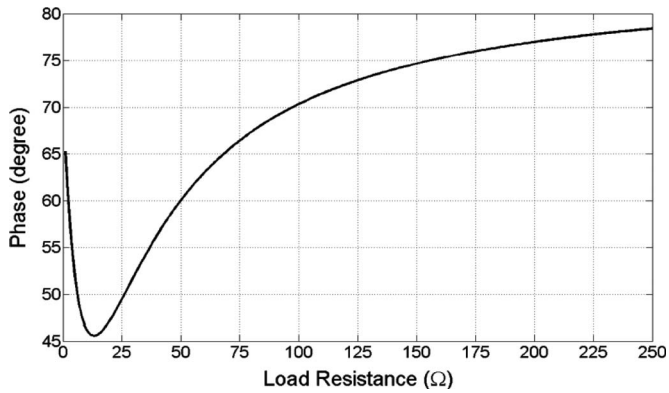

Fig. 12. Phase of Z_{tx} versus load resistance.

phase angle). From the schematic of the class-E circuit in Fig. 3, it can be deduced that most of the power loss is due to the transmitting coil and inductor parasitic resistances as they are in the path of power transfer. Therefore, one way to reduce the unloaded power loss is to use an inductor with lower parasitic resistance.

For the second constraint, the reactance of the transformed impedance must have an increasing trend with respect to the load resistance in order to achieve an increasing phase response. Harmonics rejection as well as any phase shifting to bring the impedance of the transmitter load network to the appropriate range is realized by $C_{\rm out}$ and $L_{\rm out}$. $C_{\rm out}$ and $L_{\rm out}$ are selected based on the operating frequency. Because inductors are typically larger than capacitors, it is not recommended to put more than one inductor on each channel. For the selected operating frequency, $L_{\rm out}$ is selected to be 100 μH with a parasitic resistance of 1.3 Ω at 134 kHz and $C_{\rm out}$ is selected to be 68 nF with negligible parasitic resistance.

From Fig. 9, it can be determined that C_{tx} must be at least 60 nF to ensure proper phase response. Fig. 10 shows the amplitude and phase of the unloaded Z_{tx} with different C_{tx}. Since the class-E transmitter does not work well when driving capacitive load [19] and might even result in a system failure due to heating, C_{tx} values between 44 and 93 nF should be avoided. Based on both conditions, it can be concluded that C_{tx} should be above 93 nF. Although it would be ideal to have a large C_{tx} value so that the unloaded power loss is minimized, the variation of the load network reactance decreases, as shown in Fig. 9, when the value of capacitance increases. If the variation of both resistance and reactance are small, the phase shift across the load resistance is small, resulting in little variation in the power delivery versus load resistance. If the power delivered to the receiver is not reduced to a manageable level at high load resistance, power will be dissipated in the receiving coil to create heating problems. A capacitance value of 105 nF is selected for C_{tx}.

Fig. 11 shows R_{tx} and X_{tx} while Fig. 12 shows the phase response of Z_{tx} versus load resistance. Assuming that an ideal sine-wave transmitter is driving the load network, the power transmission versus the load resistance is shown in Fig. 13, using (11). Therefore, it is critical that the power-delivery profile as shown in Fig. 13 matches the power requirement of

Fig. 13. Normalized power delivered to Z_{tx} versus load resistance when transmitter is an ideal sine-wave voltage source.

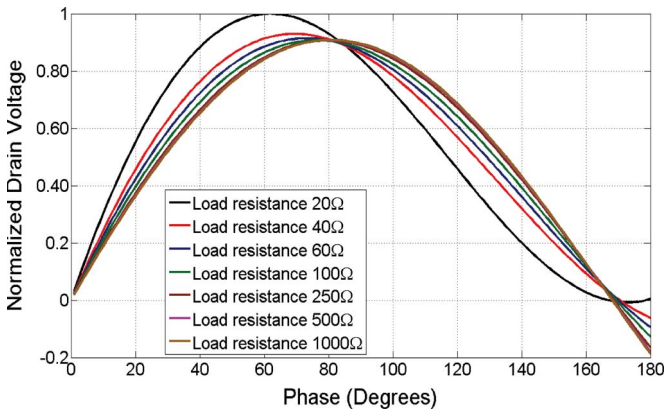

Fig. 14. Transistor drain-voltage waveform for different load resistance ($C_{\rm shunt} = 19$ nF).

the receiving device as close as possible to minimize power loss through disparity between power delivery and the power requirement.

Assuming that all of the components except the $L_{\rm out}$ and the transmitting coil are lossless and the class-E transmitter is operating in its optimal state, the power loss during the unloaded case can be approximated by

$$P = \frac{V_{CC}^2 R_{tx}}{Z_{tx}^2}. \tag{11}$$

C. Determination of $C_{\rm shunt}$ Value

Once the values of the inductors and capacitors in the transmitter load network and the receiver network are determined, the remaining step is to determine $C_{\rm shunt}$ in order to achieve ZVS and ZDS operation so as to minimize switching losses. The optimum $C_{\rm shunt}$ value can be determined using the equations derived in [19] and [20] and implemented in MATLAB code. The optimum $C_{\rm shunt}$ is found to be 19 nF, and the variation of transistor drain voltage versus load resistance is shown in Fig. 14. It can be seen that the transistor drain voltages are kept very close to zero when the transistor is being switched on at a phase of 180°. In addition, the negative voltages do not occur because the built-in diode will start to conduct and restrict the voltage at the negative of its turn-on voltage which is around −1.3 V.

TABLE I
COMPONENT VALUES

	Calculated	Experimental	% Variation
C_{rx}	113 nF	115 nF	+1.8%
Ct_x	105 nF	100 nF	-4.8%
C_{out}	68 nF	68 nF	0%
L_{out}	100 µH	100 µH	0%
L_{out} parasitic resistance	-	1.3 Ω	-
C_{shunt}	19 nF	15 nF	-21%
TX coil inductance	-	31.95 µH	-
TX coil dimension	-	21 cm x 21 cm	-
TX coil parasitic resistance	-	0.32 Ω	-
RX coil Inductance	-	12.52 µH	-
RX coil dimension	-	13cm x 13 cm	
RX coil parasitic resistance	-	0.20 Ω	-
Mutual Inductance	-	7.475 µH	-
L_{DC}	-	500 µH	-

IV. EXPERIMENTAL VERIFICATION

A dual-channel class-E transmitter test system capable of delivering nearly 300 W with a supply voltage of 120 V is fabricated using the IRFP21N60L HEXFET power MOSFET from International Rectifier. A full-wave rectifier with a shunt charge-holding capacitor at the output using MUR420 from Vishay is fabricated to convert the ac power to dc power. Since the forward-voltage drop is 0.875 V and the reverse recovery is 30 ns, power loss due to the voltage drop and reverse recovery is small as compared to the amount of power delivered to the load. Load resistance in this section is the equivalent resistance looking into the regulator or device being charged/powered as shown in Fig. 1 instead of the equivalent resistance looking into the rectifier as shown in Fig. 3. In order to reduce losses through parasitic resistance, low-loss polypropylene capacitors are used. In order to achieve a balance between size and efficiency, a 100-μH inductor (1140-101K-RC) by Bourns Jw Miller is selected for $L_{\rm out}$. Since most of the losses of the transmitter is due to the parasitic resistance of $L_{\rm out}$, a larger and more efficient inductor can be used if space permits. Table I shows the calculated value of each component with respect to the actual component value used in the experimental setup. The calculated values are initially used and further tuned to achieve optimum power delivery and efficiency across a wide range of load resistance. Most of the values follow closely to the calculated value from MATLAB. The only exception is $C_{\rm shunt}$. The main reason for such a discrepancy is that the equation used in [20] assumes the transistor to be an ideal switch. Therefore, while calculating the drain voltage, the integrated diode in the transistor was not taken into account. The other parameters of the transistor do not have any significant effect on the calculated values, since the rise and fall times of the transistor are significantly faster than the switching time, and the drain-to-source capacitance is less than 1 nF. In addition, the turn-on resistance of the transistor is extremely small. Another

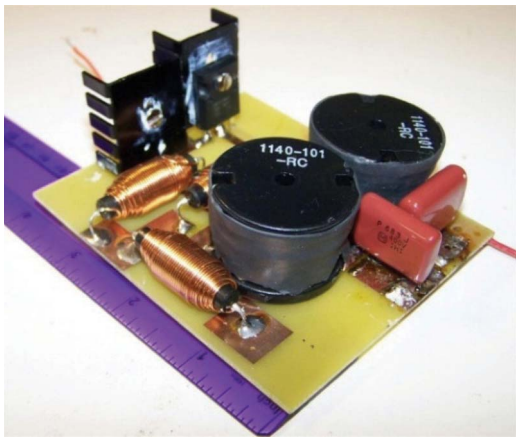

Fig. 15. Photograph of the dual-channel class-E transmitter.

reason is that, during the calculation, the dc-feed inductor $(L_{\rm dc})$ is assumed to be infinitely large, which is not true in experiment. Since the system was designed with worst case component variation of 5%, the system will perform reasonably well with components with 5% tolerance or better. A Monte Carlo analysis will be desirable but it is beyond the scope of this paper because the sensitivity also depends on the coil design. Sensitivity of the system is reduced when larger capacitance values are used. This phenomenon is shown in Fig. 5. When the value of C_{rx} increases from 100 to 150 nF, the peak resistance drops from 6 to 4 Ω. When the value of C_{rx} increases from 50 to 100 nF, the peak resistance drops from 12 to 6 Ω. Similar trend is shown in Fig. 9. The inductors $L_{\rm out}$ are placed right next to each other so that the current in both channels are "forced" to be similar due to the proximity of the magnetic field generated by the inductors, thus mitigating the variation of inductance value. The system can also be designed to be relatively insensitive to variations of $C_{\rm shunt}$. If $C_{\rm shunt}$ is smaller, the zero crossing as shown in Fig. 14 will be earlier, and it will be handled by the built-in diode of the transistor. On the other hand, if $C_{\rm shunt}$ is larger, the efficiency will be affected because the ZVS operation will not be valid, and extra power loss will incur as shown in (12). However, as long as $C_{\rm shunt}$ is not increased significantly, the drain voltage of the transistor when it is turned on will not be too large to cause device failure or significant power loss

$$P = \frac{CV_d^2 f}{2}. \tag{12}$$

The fabricated dual-channel transmitter with a dimension of 10 × 8.5 cm is shown in Fig. 15. The two inductors of $L_{\rm out}$ occupy a significant amount of space due to the requirement of low parasitic resistance to maintain high efficiency in power delivery. Fig. 16 shows the transmitting coil (21 × 21 cm) embedded inside a tabletop case and the receiving coil (13 × 13 cm) placed on top of the case. The actual separation between the two coils is 10 mm. The setup enables the user to have a large degree of translational freedom. It should be noted that there is no ferrite core in either coil.

Using a 120-V power supply, power delivery of 295 W to a 50-Ω load with a dc voltage of 121.5 V and current of 2.43 A is achieved. The input current from the power supply is

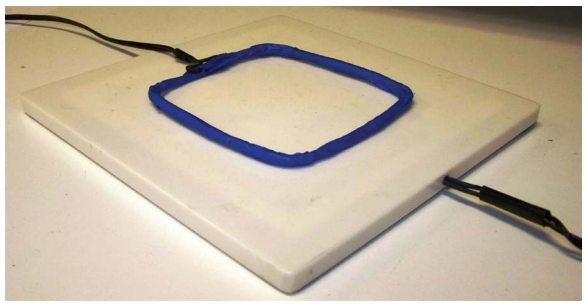

Fig. 16. Photograph of the transmitting coil—ten turns (embedded into the table top) and receiving coil—five turns (placed on top).

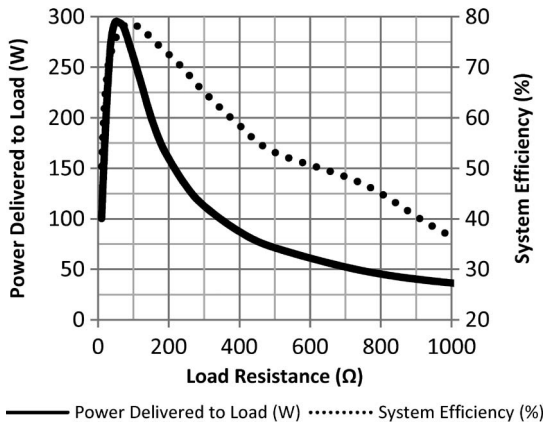

Fig. 17. (Left y-axis) Power delivery and (right y-axis) efficiency of the system versus load resistance. Supply voltage: 120 V.

3.25 A. The end-to-end system efficiency is 75.7%. Peak drain voltage is 460 V which is 25% lower than the rated maximum voltage of the transistor. Fig. 17 shows the efficiency and power delivery of the 120-V system versus load resistance. Although the maximum power of 295 W occurs at 50-Ω load resistance, a high efficiency of at least 77% is achieved across the range of 60–140 Ω, which matches the optimum range of power delivery above 200 W. The power delivered is proportional to the square of the supply voltage. The power delivery of the system can be increased by increasing the supply voltage as long as the dc-power-supply driving system is able to provide sufficient power, and the drain voltage across the transistor stays within its breakdown voltage.

The transmitter is able to operate under natural convection cooling with up to 95 W of power delivery to the load using a supply voltage of 65 V. Power levels above 95 W require forced air cooling on the transmitter to keep the temperature of the transistors below 70 °C. Although most of the loss to heat occurs at either the transistor or inductor, a temperature increase at the inductor is not critical because it is a passive component and more resilient to heat. Temperatures of both the transistor and inductor for natural convection cooling and forced air cooling were measured using the Fluke 62 mini infrared thermometer at extremely close proximity, as shown in Fig. 18. A 12-V dc dual ball-bearing fan of size 90 mm × 90 mm × 25 mm with a speed of 2700 r/min achieving an air flow of 44 $\rm ft^3/min$ is used for forced air cooling (shown in Fig. 19). In addition, the heat sinks on the transistors further

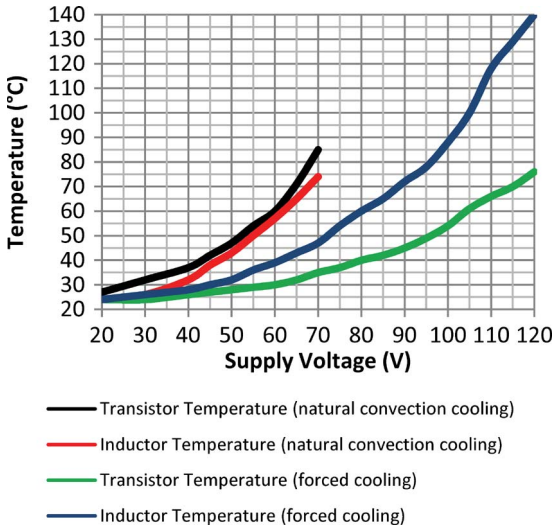

Fig. 18. Transistor and inductor temperature with natural convection cooling and forced air cooling versus supply voltage.

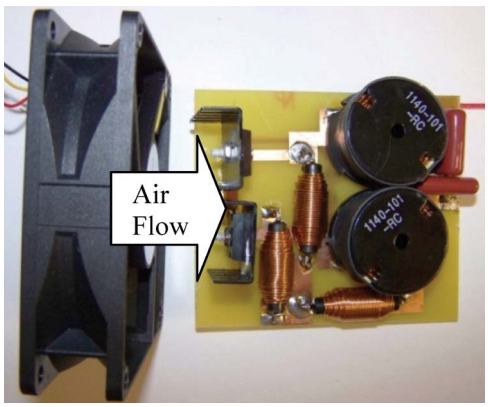

Fig. 19. Photograph of the dual-channel class E with forced air cooling.

enhance the heat-dissipation capabilities. As shown in Fig. 18, the transistor temperature reaches a practical limit of 75 °C for a supply voltage of 120 V. Although higher power can be achieved by increasing the supply voltage using a higher power-output power supply, more effective heat-dissipation methods are required to prevent the transistors from overheating.

A compact system operating without forced air cooling is often preferred. Therefore, the following measurements based on a supply voltage of 60 V operating under natural convection cooling are presented. Fig. 20 shows the transmitting-coil current and voltage when it is driving a 50-Ω load at the receiver. It can be seen that the current is lagging the voltage. As seen from the drain waveform, ZVS operation is achieved.

Fig. 21 shows the power delivery versus load resistance of both dual- and single-channel modes. The system efficiency versus load resistance is shown in Fig. 22, which matches the trend of the coupling efficiency in Fig. 7. This further verifies that the resistance looking into the network of the transmitting coil in parallel with the shunt capacitor decreases with increasing load resistance. This results in a larger voltage drop across the parasitic resistance of the inductor and a lower efficiency.

The efficiency of the single-channel mode is approximately 10%–15% lower than the efficiency of the dual-channel mode

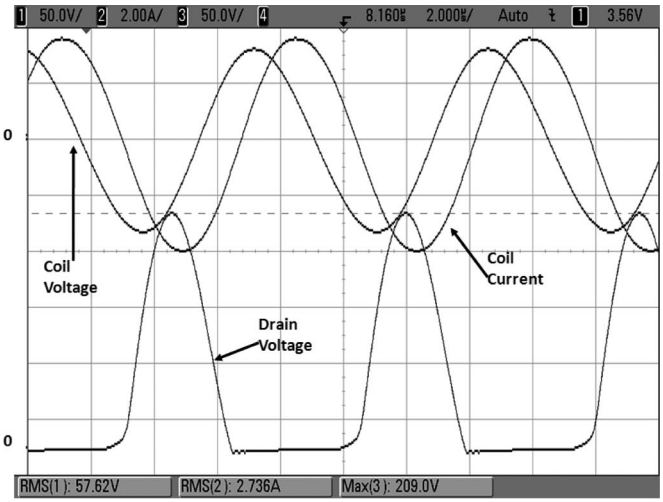

Fig. 20. Voltage and current waveforms of the class-E transmitter.

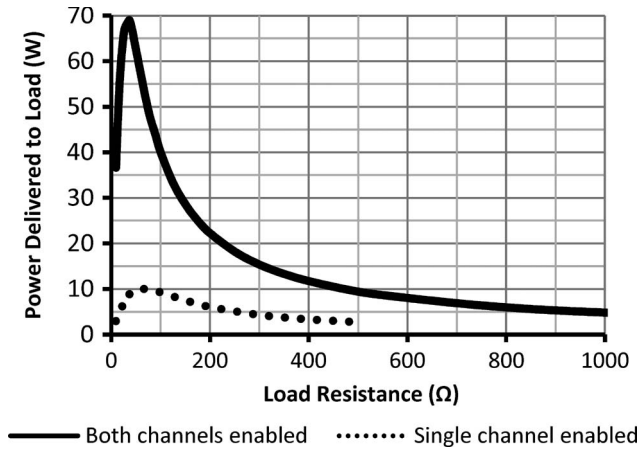

Fig. 21. Power delivered to load versus load resistance. Maximum power of 69 W occurs approximately at 50 Ω for dual-channel and maximum power of 10 W occurs at approximately at 75 Ω for single-channel. Supply voltage: 60 V.

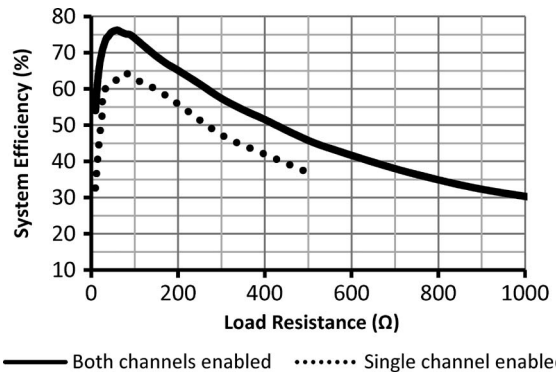

Fig. 22. System efficiency versus load resistance with a maximum efficiency of 64.5% for a single-channel system and 76% for a dual-channel system—at approximately 70 Ω. Supply voltage: 60 V.

for the same load resistance because the current is flowing through a single L_{out} inductor instead of a pair of them. This means that the parasitic resistance is doubled, thus resulting in low system and transmitter efficiencies as shown in Figs. 22 and 23, respectively. However, when the system enters

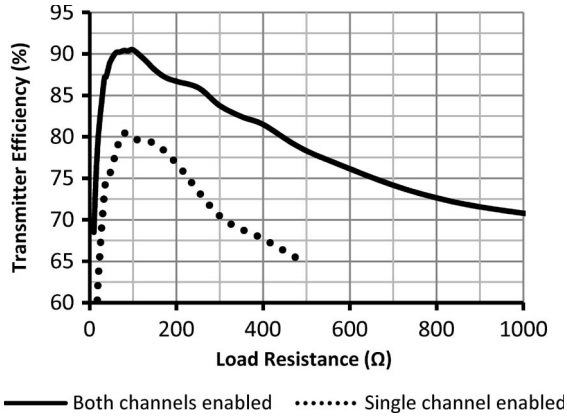

Fig. 23. Transmitter efficiency versus load resistance. Maximum transmitter efficiency occurs across the range of 60–100-Ω load resistance at 90% for dual-channel and 79% for single-channel. Supply voltage: 60 V.

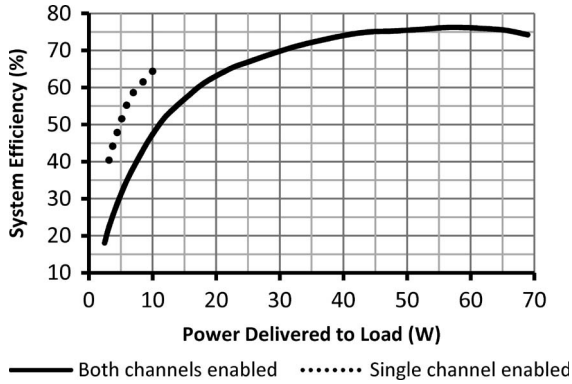

Fig. 24. System efficiency versus load resistance for single- and dual-channel modes achieving high efficiency at high-power output. It also illustrates that a single-channel mode is more efficient at low-power-delivery states. Supply voltage: 60 V.

light-load mode or trickle charge mode, it is desirable to switch to the single-channel mode. It is shown in Fig. 24 that the system efficiency is approximately 15% higher than the dual-channel mode for delivering the same amount of power below 10 W. Instead of operating at high load resistance for a dual-channel mode resulting in high receiver dc voltage as shown in Fig. 27, it is possible to achieve similar power delivery at much lower load resistance for a single-channel mode, resulting in a lower receiver dc voltage and higher system efficiency. In addition, a typical buck regulator has higher dc–dc efficiency when the input voltage is lower. Therefore, a load-detection scheme is required to determine the switch-over point from dual-channel mode to single-channel mode. It is shown in Fig. 21 that a power delivery of 10 W occurs at 500-Ω load resistance in the dual-channel mode, making it a good switch-over point to single-channel mode [Fig. 25(2)]. It is shown that a 500-Ω load resistance translates to an approximate rms voltage of 20 V across transmitting coil for the dual-channel mode as shown in Fig. 26. Likewise, if the power requirement for the single-channel mode is too high, it is required to switch to the dual-channel mode. It can be inferred from Fig. 21 that the switch-over point to dual-channel mode is approximately 75 Ω Fig. 25(4), where the efficiency peaks in single-channel mode, which translates to an rms coil voltage of 22 V in Fig. 26.

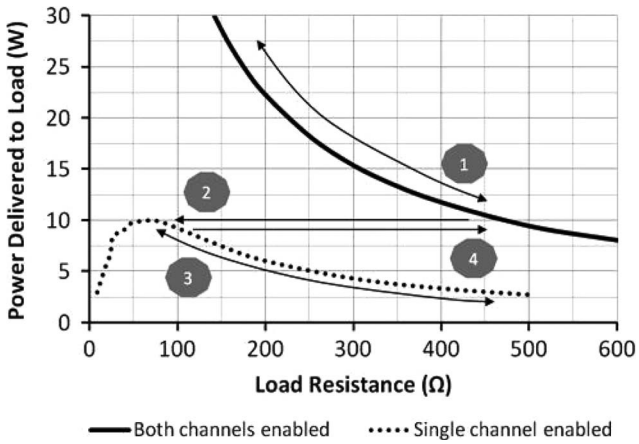

Fig. 25. Mode-switching operation for optimized efficiency across a wide power-delivery range. (1) Dual-channel mode for higher power. (2) Dual-channel mode switch-over to single-channel mode when better efficiency can be obtained at a lower power level. (3) Single-channel mode for lower power. (4) Single-channel mode switch-over to dual-channel mode when higher power delivery is needed. Supply voltage: 60 V.

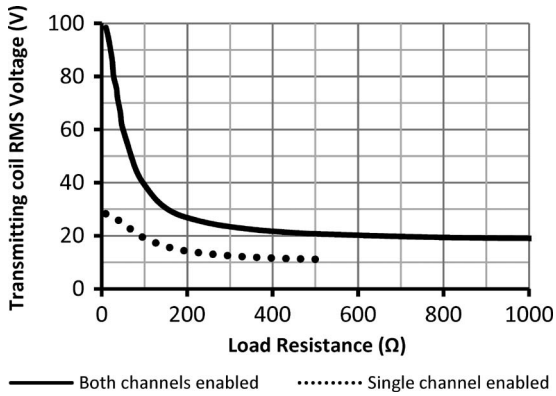

Fig. 26. Transmitting-coil rms voltage versus load resistance. Supply voltage: 60 V.

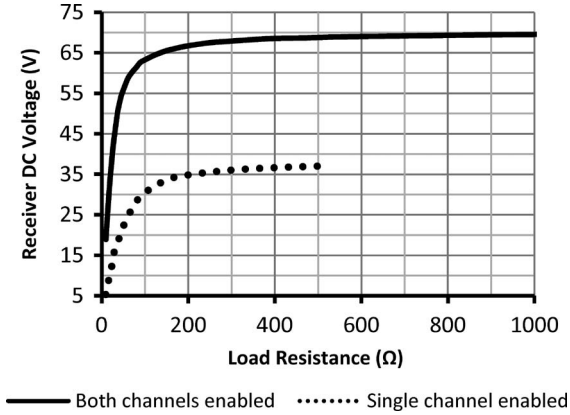

Fig. 27. Receiver dc voltage versus load resistance, converging to approximately 70 V in dual-channel mode and 37 V in single-channel mode. Supply voltage: 60 V.

Fig. 27 shows the receiver dc voltage versus load resistance. It can be seen that there is no overvoltage issue as the voltage starts to converge to a value of approximately 70 V when the load resistance is high. The receiver open-circuit voltage is 73.4 V and open-circuit power consumption is 10 W in

dual-channel mode. However, during single-channel operation, the receiver open-circuit voltage is only 38.3 V, and its open-circuit power consumption is only 4 W. Therefore, it is preferred to perform load detection using the single-channel mode and increase the output power by enabling the dual-channel mode if more power is required. By controlling the maximum receiver dc voltage, it relaxes the requirement for the receiver's regulator.

The load-detection scheme can be easily implemented by using a microcontroller with a built-in ADC. By extracting the supply current and rms voltage across the transmitting coil, the microcontroller is able to determine whether a valid receiver is placed on the transmitting coil or not.

V. Conclusion

A new technique of designing a wireless power transfer system using the class-E operation for transmission via inductive coupling has been proposed. Instead of using complex detection schemes and variable tank circuits to seek resonance and high efficiency, the system is designed to achieve the desired power-delivery profile via its natural response across a wide range of load resistances. A multichannel topology is also proposed to achieve high efficiency for different power ranges. In addition, a MATLAB program is developed to automatically generate the value for each component. Although, due to the ideal transistor and dc-feed inductor model, the generated C_{shunt} value deviates from the actual value by approximately 20%, it is close enough to perform manual optimization. Finally, a system is fabricated and tested to verify the design. The fabricated system is capable of delivering nearly 300 W with forced air cooling, and the power delivery can be varied via its supply voltage. Higher power delivery can be achieved if a power supply with higher output and transistors with higher breakdown voltages are used. With natural convection cooling, the system achieves a maximum power delivery of 69 W with end-to-end system efficiency of 74%. This is believed to be the highest power and efficiency reported for a loosely coupled wireless power transfer system with a dynamically changing load at the receiver.

Depending on the requirements, the system can be reconfigured to transmit power wirelessly to different devices for a wide variety of applications. This technology can be applied to rugged electronics to enable the creation of hermetically sealed units and to eliminate the problem of charging port contamination and corrosion. In environments where sparking and arching hazards exist, this technology can be applied to eliminate an electronic device's external metallic contacts.

References

[1] L. Collins, "Cut the cord," *Electron. Syst. Softw.*, vol. 5, no. 6, pp. 42–46, Jan.–Dec. 2007.

[2] C. E. Greene, D. W. Harrist, J. G. Shearer, M. Migliuolo, and G. W. Puschnigg, "Implementation of an RF power transmission and network," International Patent Application WO/2007/095267, Aug. 23, 2007.

[3] W. C. Brown, "The history of power transmission by radio waves," *IEEE Trans. Microw. Theory Tech.*, vol. MTT-32, no. 9, pp. 1230–1242, Sep. 1984.

[4] W. C. Brown and E. E. Eves, "Beamed microwave power transmission and its application to space," *IEEE Trans. Microw. Theory Tech.*, vol. 40, no. 6, pp. 1239–1250, Jun. 1992.

[5] *IEEE Standard for Safety Levels with Respect to Human Exposure to Radio Frequency Electromagnetic Fields, 3 kHz to 300 GHz*, IEEE Std. C95.1, 1999.

[6] R. Laouamer, M. Brunello, J. P. Ferrieux, O. Normand, and N. Bucheit, "A multi-resonant converter for non-contact charging with electromagnetic coupling," in *Proc. 23rd IEEE Int. Conf. Electron., Control Instrum.*, Nov. 1997, vol. 2, pp. 792–797.

[7] H. Abe, H. Sakamoto, and K. Harada, "A non-contact charger using a resonant converter with parallel capacitor of the secondary coil," in *Proc. IEEE Appl. Power Electron. Conf. Expo.*, Feb. 15–19, 1998, vol. 1, pp. 136–141.

[8] J. Acero, D. Navarro, L. A. Barraga, I. Garde, J. I. Artigas, and J. M. Burdio, "FPGA-based power measuring for induction heating appliances using Sigma–Delta A/D conversion," *IEEE Trans. Ind. Electron.*, vol. 54, no. 4, pp. 1843–1852, Apr. 2007.

[9] Y. Lu, K. W. E. Cheng, Y. L. Kwok, K. W. Kwok, K. W. Chan, and N. C. Cheung, "Gapped air-cored power converter for intelligent clothing power transfer," in *Proc. 7th Int. Conf. Power Electron. Drive Syst.*, Nov. 27–30, 2007, pp. 1578–1584.

[10] Y. Jang and M. M. Jovanovic, "A contactless electrical energy transmission system for portable-telephone battery chargers," *IEEE Trans. Ind. Electron.*, vol. 50, no. 3, pp. 520–527, Jun. 2003.

[11] C. Wang, G. A. Covic, and O. H. Stielau, "Power transfer capability and bifurcation phenomena of loosely coupled inductive power transfer systems," *IEEE Trans. Ind. Electron.*, vol. 51, no. 1, pp. 148–157, Feb. 2004.

[12] C. Wang, G. A. Covic, and O. H. Stielau, "Investigating an LCL load resonant inverter for inductive power transfer applications," *IEEE Trans. Power Electron.*, vol. 19, no. 4, pp. 995–1002, Jul. 2004.

[13] C. Wang, O. Stielau, and G. A. Covic, "Design considerations for a contactless electric vehicle battery charger," *IEEE Trans. Ind. Electron.*, vol. 52, no. 5, pp. 1308–1314, Oct. 2005.

[14] G. A. Kendir, W. Liu, G. Wang, M. Sivaprakasam, R. Bashirullah, M. S. Humayun, and J. D. Weiland, "An optimal design methodology for inductive power link with class-E amplifier," *IEEE Trans. Circuits Syst. I, Reg. Papers*, vol. 52, no. 5, pp. 857–866, May 2005.

[15] U. Joe and M. Hgovanloo, "Design and optimization of printed spiral coils for efficient transcutaneous inductive power transmission," *IEEE Trans. Biomed. Circuits Syst.*, vol. 1, no. 3, pp. 193–202, Sep. 2007.

[16] X. Liu and S. Y. R. Hui, "An analysis of a double-layer electromagnetic shield for a universal contactless battery charging platform," in *Proc. 36th IEEE Power Electron. Spec. Conf.*, Jun. 16, 2005, pp. 1767–1772.

[17] X. Liu and S. Y. R. Hui, "Optimal design of a hybrid winding structure for planar contactless battery charging platform," *IEEE Trans. Power Electron.*, vol. 23, no. 1, pp. 455–463, Jan. 2008.

[18] G. Gwon, D. Park, S. Choi, and S. Han, "Wireless charger decreased in variation of charging efficiency," International Patent Application WO/2007/13725, Feb. 1, 2007.

[19] F. H. Raab, "Effects of circuit variations on the class E tuned power amplifier," *IEEE J. Solid-State Circuits*, vol. SSC-13, no. 2, pp. 239–247, Apr. 1978.

[20] F. H. Raab, "Idealized operation of the class E tuned power amplifier," *IEEE Trans. Circuits Syst.*, vol. CAS-24, no. 12, pp. 725–735, Dec. 1977.

[21] J. J. Casanova, Z. N. Low, J. Lin, and R. Tseng, "Transmitting coil achieving uniform magnetic field distribution for planar wireless power transfer system," in *Proc. IEEE Radio Wireless Symp.*, Jan. 18–22, 2009, pp. 530–533.

Zhen Ning Low (S'01) received the B.Eng. degree under the accelerated bachelor program from Nanyang Technological University, Singapore, in 2005. Since 2006, he has been working toward the Ph.D. degree in the Electrical and Computer Engineering Department, University of Florida, Gainesville.

In February 2005, he was a Research Engineer with the Institute for Infocomm Research, Singapore, where he was involved in Zigbee wireless sensor networks and ultrawideband position location systems. He is currently the Team Leader of the wireless power-transmission project with the Radio Frequency Circuits and Systems Research Group. His current research interests include wireless power transmission, RF systems, microwave circuits, low-power sensor networks, and antenna design. He has authored or coauthored more than 15 technical publications in refereed journals and conference proceedings. He has filed six patent applications in the area of wireless power transmission.

Raul Andres Chinga (S'08) received the B.S. degree from the University of Florida, Gainesville, in 2008, where he is currently working toward the Ph.D. degree in electrical engineering in the Electrical and Computer Engineering Department.

His current research interests include wireless energy transmission, high-speed near-field communication, and RF system-on-chip integration.

Mr. Chinga was the recipient of the Bridge to the Doctorate Fellowship by the University of Florida in May 2008.

Ryan Tseng received the B.S. degree from the University of Florida, Gainesville, in 2006. He is currently working toward the Masters of Business Administration degree in the Sloan School of Management, Massachusetts Institute of Technology, Cambridge.

In July 2006, he founded WiPower Inc., Gainesville, FL, where he aims to develop wireless power-transmission technology and is currently the CEO of WiPower, Gainesville, FL.

Jenshan Lin (S'91–M'91–SM'00) received the B.S. degree from National Chiao Tung University, Hsinchu, Taiwan, in 1987, and the M.S. and Ph.D. degrees in electrical engineering from the University of California, Los Angeles (UCLA), in 1991 and 1994, respectively.

In 1994, he was a Member of Technical Staff with AT&T Bell Laboratories (currently, Lucent Bell Laboratories), Murray Hill, NJ, where in 2000, he became the Technical Manager of RF and high-speed circuit design research and was involved with RF integrated circuits using various technologies for wireless communications. In September 2001, he joined Agere Systems, a spin-off from Lucent Technologies. In July 2003, he joined as an Associate Professor with University of Florida, Gainesville, where since August 2007, he has been a Full Professor in the Electrical and Computer Engineering Department. His current research interests include sensors and biomedical applications of microwave and millimeter-wave technologies, wireless energy transmission, RF system-on-chip integration, and integrated antennas. He has authored or coauthored over 170 technical publications in refereed journals and conference proceedings. He is the holder of six patents.

Dr. Lin is an Associate Editor for the IEEE TRANSACTIONS ON MICROWAVE THEORY AND TECHNIQUES. He was the General Chair of the 2008 RFIC Symposium and is the Technical Program Chair of the 2009 Radio and Wireless Symposium. He was the recipient of the 1994 UCLA Outstanding Ph.D. Award, 1997 Eta Kappa Nu Outstanding Young Electrical Engineer Honorable Mention Award, and 2007 IEEE MTT-S N. Walter Cox Award.